Title

Caecilians maintain a functional long-wavelength-sensitive cone opsin gene despite signatures of relaxed selection and more than 200 million years of fossoriality

Running title

A long-wavelength cone opsin in caecilians

Authors

Maria José Navarrete Méndez[1,2,*], Sina S. Amini[1,*], Juan Carlos Santos[2], Jacob Saal[1], Marvalee H. Wake[1], Santiago R. Ron[3], and Rebecca D. Tarvin[1]

[1] Department of Integrative Biology and Museum of Vertebrate Zoology, University of California Berkeley, Berkeley, CA, USA 94720

[2] Department of Biological Sciences, St John's University, NY, USA 11439

[3] Museo de Zoología, Facultad de Ciencias Exactas y Naturales, Pontificia Universidad Católica del Ecuador, Quito, Ecuador

[*] Co-first authors

Corresponding author contact information

Rebecca Tarvin: rdtarvin@berkeley.edu

Author contributions

RDT, MJNM, SSA, JCS, SRR conceptualized the study; RDT, MJNM, SRR, SSA, JCS, MHW, JS collected data; MJNM, RDT, SSA, SSR performed analyses; MJNM, SSA, RDT, MHW, JS,

JCS, SSR performed the investigation; RDT, SRR, JCS acquired funding; SRR, MJNM, MHW contributed samples and helped with permits; MJNM, SSA, JS, MHW, JCS, RDT, SSR prepared the original draft; RDT coordinated and supervised the project; all authors reviewed and revised the manuscript.

Conceptualization	RDT, JCS, MJNM, SSA, SRR	Ideas; formulation or evolution of overarching research goals and aims.
Methodology	MJNM, RDT, SSA, JCS	Development or design of methodology; creation of models.
Software	--	Programming, software development; designing computer programs; implementation of the computer code and supporting algorithms; testing of existing code components.
Validation	--	Verification, whether as a part of the activity or separate, of the overall replication/reproducibility of results/experiments and other research outputs.
Formal Analysis	MJNM, RDT, SSA, SSR	Application of statistical, mathematical, computational, or other formal techniques to analyze or synthesize study data.

Investigation	MJNM, SSA, RDT, MHW, JS, JCS, SSR	Conducting a research and investigation process, specifically performing the experiments, or data/evidence collection.
Resources	RDT, SRR, JCS, MHW	Provision of study materials, reagents, materials, patients, laboratory samples, animals, instrumentation, computing resources, or other analysis tools.
Data Curation	--	Management activities to annotate (produce metadata), scrub data and maintain research data (including software code, where it is necessary for interpreting the data itself) for initial use and later reuse.
Writing – Original Draft Preparation	MJNM, SSA, RDT, JS, MHW, SSR, JCS	Creation and/or presentation of the published work, specifically writing the initial draft (including substantive translation).
Writing – Review & Editing	all	Preparation, creation and/or presentation of the published work by those from the original research group, specifically critical review, commentary or revision – including pre- or post-publication stages.
Visualization	--	Preparation, creation and/or presentation of the published work, specifically visualization/data

		presentation.
Supervision	RDT	Oversight and leadership responsibility for the research activity planning and execution, including mentorship external to the core team.
Project Administration	RDT	Management and coordination responsibility for the research activity planning and execution.
Funding Acquisition	RDT, SRR, JCS	Acquisition of the financial support for the project leading to this publication.

Acknowledgments. We thank Rayna Bell and Lauren Sheinberg at the California Academy of Sciences and Carol Spencer at the Museum of Vertebrate Zoology for facilitating access to caecilian tissues for sequencing. We thank José Simbaña and Yanayacu Biological Station for permission and facilitation of specimen collection, Alexander Stubbs and Diego Paucar for their assistance in caecilian dissections and specimen preparation, Todd Oakley and Seth Frazer for their support in running the machine learning models to estimate λ_{max} values for our sampled genes, Alex Somlyay for assistance with microscopy, Valeria Ramírez-Castañeda and Lydia Smith for conducting PCRs on MVZ tissues, Claudia Terán for laboratory work at QCAZ in Quito. Yocelyn Gutiérrez-Guerrero provided advice and guidance in the transcriptome analysis. For specimen collection in Ecuador, we thank William Booker, Verónica Crespo, Juan Guayasamin, Giovanna Romero, Yerka Sagredo, Scott Tiegs, and David Velalcazar. Funding was provided by Secretaría Nacional de Educación Superior, Ciencia, Tecnología e Innovación

del Ecuador SENESCYT (Arca de Noé initiative; SRR and Omar Torres principal investigators), NIH NIGMS R35GM150574 to RDT, UC Berkeley start-up funding to RDT, fellowships from the American Association of University Women and Philomathia to MJN, and long-term support from the USA National Science Foundation to MHW. The Ecuadorian Ministry of Environment provided permits for specimen collection and genetic research: 008-09 IC-FAU-DNB/MA, 005-12 IC-FAU-DNB/MA, 003-15 IC-FAU-DNB/MA, MAE-DNB-CM-2015-0025-M-0001, and MAAE-DBI-CM-2022-0230. Finally, we acknowledge and express gratitude for the animals involved in this study.

Data accessibility statement

Sequences are deposited in GenBank with accession numbers PQ541071-PQ541084 and in the Sequence Read Archive with project number PRJNA1181370. Specimens are deposited in the Museo de Zoología (QCAZ) at the Pontificia Universidad Católica del Ecuador, the Museum of Vertebrate Zoology (MVZ) at UC Berkeley, and the Herpetology Collection at the California Academy of Sciences. All other data are available as supplementary material. Upon acceptance, supplementary data will also be uploaded and archived with Data Dryad.

TITLE

Caecilians maintain a functional long-wavelength-sensitive cone opsin gene despite signatures of relaxed selection and more than 200 million years of fossoriality

ABSTRACT

Visual systems are tuned to animals' ecologies, evolving in response to specific light environments and visual needs. Ecological transitions to fossorial lifestyles impose strong selective pressures favoring morphological adaptations for underground life, such as increased skull ossification and reduced eye protrusion. Fossoriality may simultaneously relax constraints on other aspects of vision leading to diminished visual capabilities. Caecilians (Gymnophiona)—specialized, fossorial amphibians—possess reduced eyes covered by skin or bone. For years, these traits, along with the presence of a single photoreceptor expressing one functional opsin gene, have been interpreted as evidence of limited visual capabilities, including an inability to focus or perceive color. Our results challenge these assumptions: we identified the long-wavelength-sensitive (*LWS*) opsin gene in 11 species of caecilians spanning 8 of 10 recognized families. Molecular evidence indicates that *LWS* is intact and transcribed in the eye of at least one species (*Caecilia orientalis*). Anatomical observations from five caecilian families indicate highly organized retinae even in families with vestigial eyes. While the presence of cone cells in our study species remains uncertain, a putatively functional *LWS* gene suggests that the visual capabilities of caecilians and the role of light perception in their ecology may be underestimated.

KEYWORDS: visual opsins, relaxed selection, vision, OPN1LW, LWS

1. INTRODUCTION

Strong selection for adaptation to new habits, such as fossoriality, results both in gain and loss of traits (Nevo, 1979). For example, some burrowing frogs evolved spades through the enlargement of metatarsal tubercles (Emerson, 1976), yet their altered body and limbs trade off with jumping ability (Vidal-García et al., 2014). The star-nosed mole (*Condylura cristata*) evolved a novel mechanosensory structure that allows them to "see" prey (Catania, 1999; Holmberg, 2022) despite having small, underdeveloped eyes (Carmona et al., 2010). In these and other animals, subterranean life intensifies selection pressures for adaptations that facilitate life underground and relaxes selection for traits that are no longer as relevant.

Although relaxed selection can lead to trait degeneration, it is rare that traits are ever completely lost because they may be developmentally constrained, still possess some functional value, or cost little to maintain (Sadier et al., 2022). Partial eye degeneration without complete loss is a common characteristic of fossorial, deep-sea, and cave-dwelling vertebrates. For example, the European mole (*Talpa europaea*) and Iberian mole (*Talpa occidentalis*) have organized retinae with rod and cone cells despite being fully subterranean (Carmona et al., 2009; Glösmann et al., 2008); *T. occidentalis* never even opens its eyelids. Eyeless populations of the cave-dwelling fish *Astyanax mexicanus* develop a layered retina during their embryonic stage, retaining the ability to exhibit light-entrained retinomotor rhythms even as their eyes undergo extensive ontological degeneration (Emam et al., 2020; Espinasa & Jeffery, 2006).

Eye degeneration can be coupled at the molecular level with the loss of visual opsin genes that encode sensitive photoreceptor proteins (Bowmaker, 2008; Lin et al., 2024). Opsins have been lost in deep-sea fish and fossorial mammals, reptiles, and amphibians, yet they

maintain a well-developed ocular anatomy, including an organized and layered retina (Foureaux et al., 2010; Wake, 1985; Warrant, 2000). Among the four opsin gene classes, the *LWS* opsin exhibits peak sensitivity to the longest wavelengths within the visible spectrum (490–570 nm, corresponding to red-green hues) and is one of the most consistently retained across vertebrates W. I. L. Davies et al., 2012; Ford et al., 2024; Musilova et al., 2021).

Ancestors of caecilians, a group of limb-less amphibians, began their transition to a subterranean lifestyle more than 250 million years ago (MYA) through elongation of the trunk, fusion of cranial bones, and reduction of limbs (Jenkins & Walsh, 1993; Santos et al., 2020). In extant caecilians (Order Gymnophiona, with most recent common ancestor 190 MYA; Kligman et al., 2023), all species lack limbs, have eye sockets that are covered by skin or by skin and bone, and lack the eye muscles for accommodation (Wake, 1985). Many species have lost one or more of the extrinsic eye muscles, several taxa have aborted lens development, and a few have lost the lens completely; several have reduced organization of the retina, and reduced numbers of cells (Wake, 1985). In spite of these constraints, evidence from anatomy, physiology, and molecular biology has shown that visual systems in caecilians have remained somewhat functional (Dünker, 1998; Mohun et al., 2010; Mohun & Wilkinson, 2015; Wake, 1985). Although caecilian retinae are thought to lack cone cells, a gene encoding a cone opsin was recently discovered in a few published genomes (Lin et al., 2024).

Here we aimed to characterize the evolution of visual opsin genes in caecilians, which might shed light on their function and explain why a long-wavelength-sensitive opsin has been maintained for many millions of years despite degeneration of the eye, including the apparent loss of cone cells. We also provide an updated anatomical review of caecilian retinae, eye

musculature, and eye exposure based on the modern phylogenetic understanding of the group, including a set of images of caecilian retinae representing five families.

2. METHODS

2.1 COMPILATION AND REVIEW OF EXISTING *LWS* DATA

2.1.1 Review of prior evidence suggesting loss of LWS. A previous attempt to amplify *LWS* (also known as *OPN1LW*) from two species of caecilians (*Ichthyophis* cf. *kohtaoensis* and *Typhlonectes natans*) using eye cDNA from adult specimens was unsuccessful (Mohun et al., 2010). Given that previous work reported a putatively functional copy of *LWS* in three other species of caecilians (Lin et al., 2024), we wanted to verify whether a mismatch between primer and template could have resulted in a failed PCR. Thus, we used the 'water' local alignment tool from EMBOSS (Rice et al., 2000), which implements the Smith-Waterman algorithm, to review potential alignments between primers from Mohun et al. (2010) and cDNA sequences of three published caecilian *LWS* genes (*Rhinatrema bivittatum*, XM_029609805.1; *Microcaecilia unicolor*, XM_030192059.1; *Geotrypetes seraphini*, XM_033922369.1). We report values for forward primers aligned to the forward sequence and for reverse primers aligned to the reverse complement of the sequence.

2.1.2 Analysis of the synteny of LWS in amphibians and genome mining in caecilians. The visual opsin genes *LWS* and *SWS2* are in a tandem arrangement on the same chromosome in many vertebrates (W. I. L. Davies et al., 2012). We took advantage of this arrangement to search for *LWS*, corroborate the absence of *SWS2*, and investigate the possibility of a pseudogenized version of *SWS2* in the publicly available caecilian genomes. We expected that if *SWS2* is lost, it

would still be possible to detect remnants of the gene in the genomic data, appearing as a pseudogene either near its original location, upstream of *LWS*, or moved to a different region within the genome. We also included other upstream genes known to be part of this synteny block: *HCFC1* (host cell factor C1), *TMEM187* (transmembrane protein 187), *IRAK1* (interleukin 1 receptor-associated kinase 1) and *MECP2* (methyl-CpG binding transcription factor).

We retrieved annotated scaffolds containing *HCFC1–LWS* of three caecilian species: *Microcaecilia unicolor* (GCF_901765095. 1), *Geotrypetes seraphini* (GCF_902459505.1), and *Rhinatrema bivittatum* (GCF_901001135.1), and three anuran species: *Xenopus tropicalis* (GCF_901001135.1), *Nanorana parkeri* (GCF_000935625.1), and *Bufo bufo* (GCF_905171765.1) from NCBI (Supplementary Table 1). Sequences were aligned using MAFFT v7.490 (Katoh & Standley, 2013) and visualized in Geneious Prime 2022.1.1 (https://www.geneious.com). To evaluate and visualize the evolutionary dynamics of the *HCFC1–LWS* syntenic arrangement within the examined amphibian genomes, we organized our alignment using a calibrated phylogeny generated by TimeTree (Kumar et al., 2022). The topology depicted by TimeTree and the calibration times are consistent with ages estimated using fossil calibrations (Kligman et al., 2023).

Finally, we mined the genomes of four caecilian species to search for *LWS, RH1, SWS2, SWS1*, or remnants of these genes: *Rhinatrema bivittatum*, *Microcaecilia unicolor* , *Geotrypetes seraphini* and *Ichthyophys bannanicus* (GCA_033557465, hereafter *I. kohtaoensis* following Nishikawa et al., 2021). This approach complemented our search for *SWS2* accounting for the case that the synteny relationship between *SWS2* and *LWS* was disrupted in caecilians, potentially locating the *SWS2* gene elsewhere in the genome.

2.2 FURTHER VALIDATION OF A CAECILIAN *LWS*

2.2.1 Generating an eye transcriptome. To further interrogate the possible function (or lack thereof) of *LWS*, we collected one *Caecilia orientalis* in 2020 at Yanayacu Biological Station in Napo, Ecuador (S 0.5984097, W 77.8907409, 2143 m.a.s.l.) under collection permit Contrato Marco Acceso a los Recursos Genéticos MAE-DNB-CM-2015-0025-M-0001 issued by the Ministerio del Ambiente, Agua y Transición Ecológica of Ecuador to Pontificia Universidad Católica del Ecuador.

We euthanized the specimen using commercial Roxicaine anesthetic spray (lidocaine) and immediately dissected both eyes which were preserved in RNAlater for transcriptomic analysis. The specimen is archived in the herpetological collection at Museo de Zoología of the Pontificia Universidad Católica del Ecuador (QCAZ), with specimen number QCAZ:A:77338. Tissue samples were sent to Macrogen Inc. (Seoul, South Korea) for RNA extraction, library preparation using the Illumina TruSeq Stranded mRNA LT Sample Preparation Kit, and sequencing on the Illumina NovaSeq6000 to 100 million paired-end 100-bp reads.

Read quality was assessed using FastQC (Andrews, 2010). We used TrimGalore! (https://www.bioinformatics.babraham.ac.uk/projects/trim_galore/) to remove adapters, low-quality bases, and short reads. Transcriptome assembly was then conducted *de novo* using Trinity v2.13.2 (Grabherr et al., 2011), incorporating all paired-end reads with default settings. The resulting assembly was filtered using SeqClean (Chen et al., 2007). To annotate protein-coding genes, TransDecoder v2.026 (Haas, n.d.) was used with default parameters and homology to UniProt was then used to infer functions of predicted genes with NCBI-BLASTP v2.2.30+ (E-value = 1e−6) and Interproscan 5.35 (Jones et al., 2014) to detect proteins with known functional

domains. Finally, we used Salmon v1.10.3 (Patro et al., 2017) to quantify transcript abundances of opsin genes. First, we built a Salmon index for our transcriptome using the index command with default parameters for k-mer length. Next, we quantified the paired-end reads against the previously generated index using the quant command. The output gene counts were summarized as normalized transcript abundances using DESeq2 v3.11 (Love et al., 2014).

2.2.2 PCR of* LWS *in additional caecilian species. To validate whether *LWS* existed in a broader phylogenetic sampling of caecilians, we obtained tissue samples from *C. orientalis*, *Epicrionops bicolor*, *Epicrionops petersi*, and *Microcaecilia albiceps* from specimens housed in QCAZ. Tissues from *Dermophis mexicanus*, *G. seraphini*, *Gymnopis multiplicata*, *I. kohtaoensis*, and *Typhlonectes natans* were obtained from the Museum of Vertebrate Zoology (MVZ) at the University of California, Berkeley. Tissues from *Boulengerula boulengeri* and *Scolecomorphus vittatus* were kindly loaned from the California Academy of Sciences. See Supplementary Table 1 for accession numbers.

DNA extraction, amplification, and sequencing was carried out at PUCE for QCAZ specimens, and at the Evolutionary Genomics Lab (EGL), UC Berkeley, for MVZ and CAS specimens. For the QCAZ samples, DNA was extracted from liver or muscle tissues preserved in 95% ethanol, following standard guanidine thiocyanate extraction protocols. DNA from MVZ and CAS samples was extracted from liver or muscle preserved in 95% ethanol by salt extraction.

Fragments of *LWS* were amplified using new primer sets designed from an alignment of amphibian opsins. The new LWS_542R (5’-GCA GAC CAA ACC CAG GAG AA-3’) and LWS_117F (5’ TTT TGA GGG MCC CAA CTA CC -3’) primers amplify a region that includes part of exon I, the intron between exon I and II, and part of exon II. PCR conditions were as

follows: denaturation at 94˚C for 2 min, followed by 38 amplification cycles (94˚C for 30 s, 54˚C for 30 s, 72˚C for 1 min), and a final extension at 72˚C for 7 min. Resultant amplicons were purified with ExoSAP-it (Applied Biosystems; Waltham, Massachusetts). PCR products from QCAZ samples were sequenced at Macrogen Inc. (Seoul, South Korea); MVZ and CAS samples were sequenced at the UC Berkeley DNA Sequencing Facility. We assembled forward and reverse sequences into consensus sequences using default parameters in Geneious Prime 2022.1.1 and then aligned them against each other using MUSCLE (Edgar, 2004).

To confirm the identity and quality of the new *LWS* sequences, we inferred gene trees for *LWS* and *RH1* in IQTREE2. Sequences were partitioned by coding and non-coding regions and also by codon position. The best-partition model was estimated using the -TESTMERGE option (Chernomor et al., 2016; Kalyaanamoorthy et al., 2017). Bootstrap values were calculated using 500 replicates (-b 500) and were plotted on the best likelihood tree. See Supplementary Material Data 1 for input and output files.

***2.2.3 Estimation of the wavelength of maximum absorbance (λ_{max}) of* LWS *and* RH1.** We used a machine-learning model (Frazer et al., 2024) to estimate the wavelength of maximum absorbance (λ_{max}) for five full-length *LWS* and *RH1* sequences from the caecilian species included in our study including the species available in GenBank (*G. seraphini*, *I. kohtaoensis*, *M. unicolor*, and *R. bivittatum*) and from our *C. orientalis* eye transcriptome. Additionally, we increased our phylogenetic sampling by including *LWS* and *RH1* sequences from other relevant amphibian and vertebrate species. For this purpose, we explored three types of sequence archives: NCBI sequence references, unannotated transcriptomes, and published genomes. Sequences were identified as *LWS* orthologs if they closely matched the Gymnophiona reference for *Microcaecilia unicolor OPN1LW* (XM_030192059.1). Homology was assessed using

BLAST+, and sequences were included if they contained all six exons (as in the human *OPN1LW* gene, NM_020061.6) or if most exons had e-values of $<10^{-20}$. The methods used to retrieve *LWS* from each of these datasets are described in more detail in the Supplementary Material Section 2. Our final dataset included 19 species of Anura and 8 species of Urodela (see Supplementary Table 1 for details). The nucleotide matrices were manually inspected to remove any ambiguities and the sequences were translated to amino acids for downstream analysis.

Point estimations of λ_{max} for *LWS* and *RH1* were predicted using the vertebrate model trained with the VPOD_vert_het_1.0 dataset available in the Visual Physiology Opsin Database (https://github.com/VisualPhysiologyDB/visual-physiology-opsin-db). This model demonstrated the best predictive ability, with the highest 10-fold cross-validation R^2 (0.968) and the lowest mean absolute error (6.56 nm) among all the models compared in the machine learning analysis (Frazer et al., 2024). The VPOD_vert_het_1.0 dataset comprises 721 vertebrate opsins genes (13 UVS, 167 SWS, 8 MWS, 83 LWS, 237 RH1, and 113 RH2) including wild-type, mutant, and chimeric opsins with λ_{max} ranging from 350 to 611 nm.

Additionally, a literature search was conducted to identify available microspectrophotometry (MSP) data for the species included in our machine-learning analysis. In some instances, when values were not available for a particular species, we used data from a closely related species within the same genus (Supplementary Material Table 5). We then performed a direct comparison between the MSP data and the machine-learning estimations using a linear correlation analysis (Pearson's correlation) using the lm and cor test functions in Rstudio v2024.9.1.394 and calculated the mean absolute error to quantify the discrepancy between the absorbance values obtained from the two methodologies.

2.3 SELECTION ANALYSES

We aimed to assess patterns of selection on *LWS* and *RH1* in Gymnophiona using the sequence data described in section 2.2.3. Additionally, we incorporated sequences from the *C. orientalis* transcriptome, along with fragments of exon I and exon II of *LWS* obtained through Sanger sequencing for 13 caecilian species (Supplementary Table 1). An updated and unrooted version of the phylogenetic tree presented by (Jetz & Pyron, 2018) served as a backbone for conducting selection analysis in the codeml program of PAML v4 (Yang, 2007).

Sequences for *LWS* and *RH1* were aligned using MAFFT (Katoh & Standley, 2013) followed by manual editing to remove terminal stop codons in Mesquite v3.6 (Maddison & Maddison, 2015). For *LWS*, we ran analyses on two types of datasets, a complete dataset including the full coding sequence of the gene with smaller sampling for Gymnophiona (368 aa; Anura = 19 spp, Urodela = 8 spp, Gymnophiona = 5 spp) and an incomplete dataset with more species for Gymnophiona but fewer sites (132 aa; Anura = 19 spp; Urodela = 8 spp, Gymnophiona = 13 spp). For *RH1*, we only ran analyses using the complete sequences (354 aa; Anura = 18 spp, Urodela = 6 spp, Gymnophiona = 5 spp).

We inferred phylogeny-wide selection patterns and tested for site-specific positive selection for each gene comparing the support for different models (M0, M1a, M2a, M2a_rel, M3, M7, M8a, and M8). We used the Bayes Empirical Bayes (BEB) approach to identify individual sites with a posterior probability >90% of being in the positively selected class of sites. Additionally, we compared the fit of clade models C and D (CmC vs. CmD) (Bielawski & Yang, 2004) to M3 and M2a_rel to investigate long-term shifts in selection pressures associated with the evolution of fossoriality in caecilians (Weadick & Chang, 2012). Both clade models assume three site classes, with the final class modeling divergent selection among clades. CmD

does not constraint the ω estimates for any of the site classes, while CmC does. The best model was identified using likelihood ratio tests (LRTs) with a χ^2 distribution.

Additionally, we conducted a series of analyses in HYPHY, implemented on the Datamonkey web server (Delport et al., 2010). FEL (Fixed Effect Likelihood; Kosakovsky Pond & Frost, 2005) and FUBAR (Fast, Unconstrained Bayesian AppRoximation; Murrell et al., 2013) were employed to estimate positive or purifying selection across sites by comparing single estimates of dN and dS values for each site. FUBAR uses a hierarchical Bayesian method rather than maximum likelihood, making it more sensitive than FEL to weaker signatures of positive selection (i.e., when ω is close to 1) (Murrell et al., 2013). We used BUSTED (Branch-site Unrestricted Statistical Test for Episodic Diversification; Murrell et al., 2013) to identify episodic positive selection at a fraction of sites. BUSTED allows for branch-to-branch variation across the entire phylogeny. Furthermore, we ran RELAX (Wertheim et al., 2015) to detect relaxation of selective constraint. This methodology requires an *a priori* specification (e.g., partition) of a subset of branches into foreground and background. In our case, the foreground comprised the crown Gymnophiona and its stem branch, while anurans and urodeles were designated as the background. Furthermore, RELAX uses three site classes partitioned between the foreground (test) and background (reference) branches under the constraint that ω foreground = ω background^k. The exponent k is the selection intensity parameter, where a $k < 1$ indicates a relaxation of selection (values of ω move toward 1, becoming smaller if $\omega > 1$ and larger if $\omega < 1$). In contrast, a $k > 1$ indicates an intensification of selection (values of ω move away from 1).

We report results from the selection analyses using amino acid site numbers based on bovine rhodopsin (NP_001014890.1; alignments with bovine rhodopsin are available in the Supplementary Data 2). Selection results are reported by referring to the location of each amino

acid according to the 3D structure of opsins, which encompasses seven transmembrane domains (TMD I–VII), three extracellular domains (ECD I–III), and the amino- and carboxyl- termini (N and C) (Palczewski et al., 2000).

2.4 MORPHOLOGY

2.4.1 Histology. Whole heads of adult specimens fixed in neutral buffered formalin and preserved in 70% ethanol were demineralized in 10% formic acid, embedded in paraffin, sectioned frontally or sagittally, mounted on numbered slides, stained alternately with hematoxylin-eosin, picro-ponceau, and Mallory's or Heidenhain's azan or Mallory's trichrome stains (Humason, 1979), cover slipped, boxed, and stored. The examined sections are archival material accessioned in the MVZ that were originally prepared by MHW in the 1980s (see Supplementary Material Table 2 for accession information; Wake, 1985).

2.4.2 Photomicrography. Specimen slides were observed under a digital microscope, where we sought eye sections with intact photoreceptors and retina. Photomicrography was performed using the 10x, 40x, and 100x objectives, the last of which required oil immersion. Photographs were taken at 100x, 400x, and 1000x magnifications using a Laxco SeBaCam digital microscope camera, and rendered using SeBaView software v3.7 (Laxco, Inc.). A stage micrometer was used for measurements and to calibrate scale bars.

2.4.3 Quantitative and qualitative aspects of the retina. Slides of *Epicrionops sp*., *Typhlonectes compressicauda, Ichthyophis kohtaoensis, Dermophis mexicanus,* and *Scolecomorphus kirkii* specimens were selected to highlight taxonomic and morphological diversity of retinae across Gymnophiona. Measurements (inner and outer segment lengths of photoreceptors; inner and outer plexiform layer widths) were taken with a stage micrometer. The number of rows of nuclei in the outer nuclear layer (ONL), inner nuclear layer (INL), and

ganglion cell layer (GCL) were counted. Given that the sections used are historical and represent both sagittal and frontal sections, consistency in the condition of specimens at the time of embedding and sectioning cannot be guaranteed, nor was it possible to make measurements from a standardized reference point. Instead, representative images which contained the largest cross section of the eye while showing good preservation of retinal morphology were selected for cell counts and measurements of retinal layers. Measurements are sometimes given in ranges to account for variation in cell size and spatial variation across the retina. Multiple slides flanking the selected sections and multiple specimens of the same species (when available) were examined to ensure consistency in measurements.

2.4.4 Ancestral character state reconstruction. We estimated ancestral character states for anatomical features of the eye using character data from Wake (1993), Taylor (1968, 1969), and Maciel and Hoogmoed (2011). The reconstructions were performed using stochastic character mapping in *phytools* v2.0 (Revell, 2024) on the San Mauro et al. (2014) phylogeny. Taxon sampling between Wake (1993) and San Mauro (2014) largely overlaps. However, in *Uraeotyphlus* we coded *U*. cf. *oxyurus* and *U. gansi* using *U. narayani* (Wake, 1993). We reconstructed two characters. First, eye musculature, with six discrete states: (0) all muscles lost, (1) two muscles present (rectus superior, rectus inferior), (2) three muscles present (rectus superior, rectus inferior, rectus internus), (3) four muscles present (rectus superior, rectus inferior, rectus internus, rectus externus), (4) six muscles present, with superior oblique attenuate, (5) six muscles present. This character was reconstructed under three models: equal rates, all rates different, and ordered. The second character was eye exposure, with three discrete states: (0) eye exposed, (1) eye under skin, (2) eye under bone. In *Oscaecilia ochrocephala*, the eyes are covered by bone only in adults, and some individuals can have bone covering one eye

only (MHW, pers. obs.). Similarly, *C. gracilis* eyes are not usually covered by bone, but some individuals can have one or both eyes covered by bone (Maciel & Hoogmoed, 2011). We scored both species as (2), because we considered that bone covering the eyes, at any life stage, was indicative of decreased visual function. *Scolecomorphus vittatus* lacks bony orbits and their eye is attached to the tentacle; they were coded as (1) following Wake (1993). This character was reconstructed under two models: equal rates and all rates different. In both characters, models were compared using AIC and then fitted to the stochastic mapping function according to their weight (*simmap* function). The data were plotted using *phytools* v2.0 (Revell, 2024). Information on the character states for each individual included in our analysis is provided in Supplementary Material Table 3.

RESULTS

3.1 RETRIEVAL OF *LWS* FROM CAECILIANS

We retrieved *LWS* sequences from four species of Gymnophiona (*Rhinatrema bivittatum*, XM_029609805.1; *Microcaecilia unicolor*, XM_030192059.1; *Geotrypetes seraphini*, XM_033922369.1; *Ichthyophis kohtaoensis*, GCA_033557465.1). The sequences are publicly available in GenBank from Torres-Sanchez et al. (2019) and early results from the Vertebrate Genome Project ([https://vertebrategenomesproject.org/]; (Haussler et al., 2009)). In agreement with Lin et al. (2024), the other cone opsins in Urodela and Anura (Musser & Arendt, 2017), *SWS1* and *SWS2*, were not detected in these caecilian genomes.

We found that the degenerate primers used by Mohun et al. (2010) to amplify opsin genes did not align well to *LWS* sequences from caecilian genomes. Specifically, no set of primers aligned with greater than 73.0% average identity or 79.1% similarity to coding sequences (Table 1). Moreover, some alignments had large gaps (1.1–15.7%). In contrast, our primers had upwards of 95% identity with 0.0% gaps.

TABLE 1. Local alignments between *LWS* primers (Mohun et al., 2010) and published *LWS* sequences from three species of caecilians show substantial mismatch between primer and coding sequences. In contrast, primers designed for this study were more similar to published *LWS* sequences.

Primer Pair	**Alignment**	***G. seraphini***	***M. unicolor***	***R. bivittatum***	**Average**
LWS_117F/542R (this study)	% Identity	95.0/90.0	95.0/100.0	95.0/100.0	95.8
	% Similarity	100.0/90.0	100.0/100.0	100.0/100.0	98.3
	% Gaps	0.0/0.0	0.0/0.0	0.0/0.0	0.0
AMPHLWF1/R1	% Identity	57.1/70.0	54.8/73.7	56.8/80.0	65.4
	% Similarity	64.3/80.0	61.3/83.3	59.5/90.0	73.1
	% Gaps	21.4/0.0	19.4/0.0	29.7/0.0	11.8
AMPHLWF2/R2	% Identity	40.4/72.4	63.3/72.4	66.7/72.4	64.6
	% Similarity	44.2/75.9	70.0/79.3	74.1/86.2	71.6
	% Gaps	50.0/10.3	0.0/0.0	3.7/0.0	10.7
AMPHLWF3/R3	% Identity	71.0/77.8	67.6/74.1	73.3/74.1	73.0
	% Similarity	74.2/85.2	70.6/81.5	76.7/81.5	78.3
	% Gaps	6.5/3.7	14.7/3.7	0.0/3.7	5.4
AMPHLWF4/R4	% Identity	74.1/72.4	74.2/70.0	74.2/72.4	72.9
	% Similarity	81.5/75.9	80.6/76.7	80.6/79.3	79.1
	% Gaps	0.0/0.0	3.2/0.0	3.2/0.0	1.1

ALLOPSINF1/R1	% Identity % Similarity % Gaps	53.3/58.1 63.3/64.5 0.0/12.9	53.3/64.3 63.3/78.6 0.0/0.0	56.7/64.3 66.7/78.6 0.0/0.0	58.3 69.2 2.2
ALLOPSINF2/R2	% Identity % Similarity % Gaps	43.8/69.2 52.1/80.8 39.6/0.0	41.7/61.5 50.0/73.1 39.6/0.0	52.9/69.2 64.7/80.8 14.7/0.0	56.4 66.9 15.7

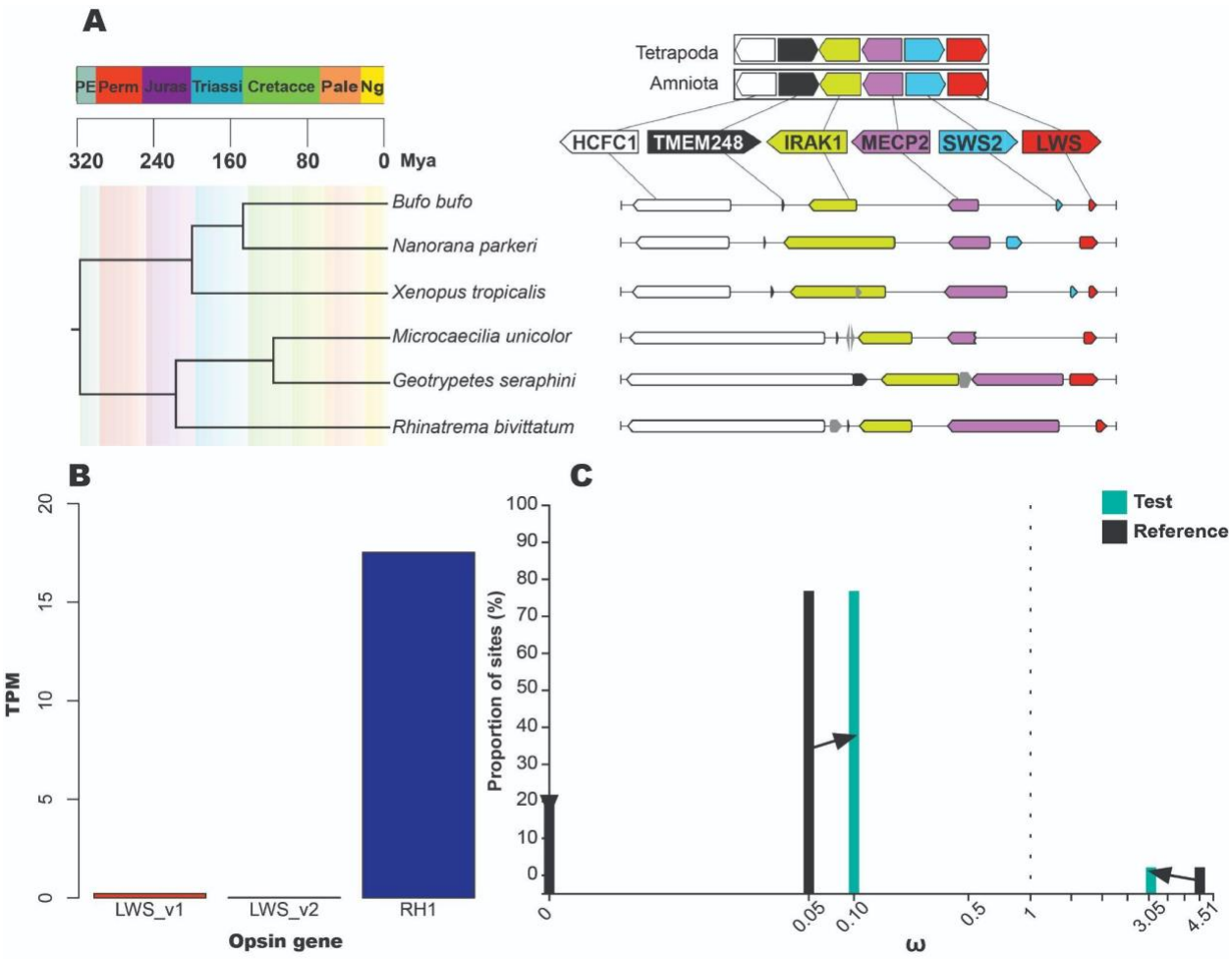

FIGURE 1. A) The *HCFC1–LWS* syntenic arrangement, which contains two opsin genes (*SWS2* and *LWS*), is conserved in the ancestors of all Tetrapoda and Amniota. Four genes are located

upstream of *SWS2* and *LWS*: *HCFC1*, *TMEM248*, *IRAK1*, and *MECP2*. This syntenic structure is preserved in the anurans *Bufo bufo* (chromosome 8, NC_053396: 25958438–26333531, Bufonidae), *Nanorana parkeri* (unplaced scaffold, NW_017306743:514864–800415; Ranidae), and *Xenopus tropicalis* (chromosome 8, NC_030684: 32111640–32353756, Pipidae), as well as in the caecilians *Microcaecilia unicolor* (chromosome 2, NC_044032: 265707065–265007887, Caecilidae), *Geotrypetes seraphini* (chromosome 1, NC_047084: 458134825–457750303, Caecilidae), and *Rhinatrema bivittatum* (chromosome 1, NC_042615:501485709–500871805, Rhinatrematidae). However, *SWS2* is absent in the scaffolds of all three caecilian genomes. A dated phylogeny from TimeTree (Kumar et al., 2022) suggests that *LWS* has been retained in these fossorial species for approximately 240 million years, while *SWS2* appears to have been lost for a similar period of time. B) Expression levels of two putative isoforms of *LWS* (*LWS_v2* lacks exon 5) and *RH1* from the eye transcriptome of *Caecilia orientalis*. Read counts are normalized as transcripts per million (TPM). C) Results from the RELAX selection analysis indicate that *LWS* in caecilians is undergoing a shift in selective pressure compared to other amphibians (see Supplementary Material File 1). The estimated ω (omega) values for the test group (Gymnophiona, shown in turquoise) compared to the reference group (Anura + Urodela, shown in black) in both ω classes ($\omega < 1$ and $\omega > 1$) are trending toward 1, as indicated by the black arrows. This analysis was performed using the complete dataset (368 amino acids; Anura = 19 species, Urodela = 8 species, Gymnophiona = 5 species).

3.2 FURTHER VALIDATION OF A CAECILIAN *LWS*

3.2.1 Transcriptomics. In total, we obtained 131,623,768 reads from *C. orientalis* eye tissue (PRJNA1181370). The reads were assembled into a reference eye transcriptome containing 175,181 transcripts. For *RH1*, one transcript was assembled, while for *LWS*, two were

assembled. Compared to *LWS_v1*, *LWS_v2* is missing exon 5. We found that *RH1* was expressed at much higher levels compared to *LWS_v1* or *LWS_v2* (80.3X and 818.5X, respectively). No sequences for *SWS1* or *SWS2* were assembled.

3.2.2 PCR. We obtained 568 bp of *LWS* sequences from 11 species of caecilians. After aligning with *C. orientalis*, all sequences had open reading frames that lacked stop codons (Supplementary Data 3).

***3.2.3 λ_{max} of* LWS *and* RH1.** The estimated λ_{max} for the complete *LWS* gene sequences of five caecilian species (*G. seraphini, I. kohtaoensis, M. unicolor, R. bivittatum*, and *C. orientalis*) ranged from 508.57 to 550.58 nm. The shortest predicted absorbance value corresponds to *LWS_v2* from *C. orientalis*. The predicted λ_{max}values for *RH1* in caecilians, using the complete gene sequences, ranged from 492.07 to 513.54 nm (Figure 2; Supplementary Material Table 5).

We estimated absorbance values for *LWS* and *RH1* in 39 additional vertebrate species, with *LWS* values ranging from 531.39 nm in the lungfish *Protopterus annectens* to 565.3 nm in the chicken *Gallus gallus*, and *RH1* values ranging from 493.72 nm in the lizard *Pogona vitticeps* to 513.54 nm in the frog *Scapiophus couchii* (Supplementary Material Table 5).

Of the 44 species we reviewed, microspectrophotometry (MSP) data were available for 14 *LWS* sequences and 21 *RH1* sequences, including for two caecilian species. Our results suggest a weak relationship between the λ_{max} values estimated using machine learning and experimental MSP data from the literature, particularly for *LWS* (Pearson's correlation: $r = 0.13$, $P = 0.66$). Although not significant, the correlation is stronger for *RH1* ($r = 0.38$, $P = 0.09$; Figure 2B). Additionally, the machine-learning estimates showed greater discrepancies from MSP data for *LWS* (mean absolute error: 26.4 nm) compared to *RH1* (2.8 nm). For the two caecilian species with *RH1* MSP data, the difference between MSP and machine learning data

was ~3 nm (Figure 2A; Supplementary Material Table 5); MSP data for *LWS* was not available to compare.

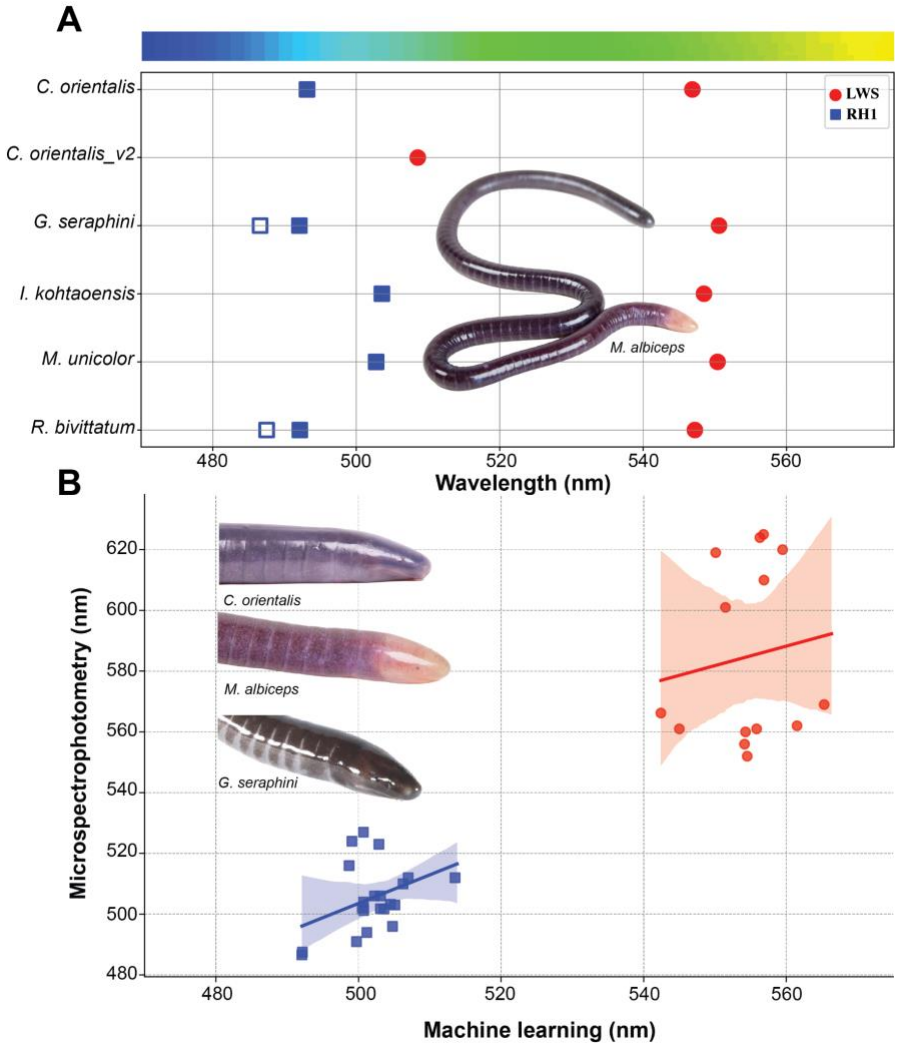

FIGURE 2. A) Maximum wavelength absorbance values (λ_{max}) for *LWS* and *RH1* estimated using a regression-based machine learning model (ML; solid markers; Frazer et al., 2024) or microspectrophotometry (MSP; hollow markers; Mohun et al., 2010) for five caecilian species. Because *LWS* was previously thought to be absent in caecilians, no MSP data is available for this opsin. The color scale at the top of the figure represents the visible light spectrum for the range

of estimated absorbance values (470–570 nm). The image corresponds to *Microcaecilia albiceps*. B) Linear regression between ML and MSP data for *LWS* (Pearson's correlation test: $r = 0.13$, $P = 0.66$) and *RH1* ($r = 0.38$, $P = 0.09$). The images show three caecilian species included in our study: *C. orientalis*, *M. albiceps* (© Santiago Ron; BIOWEB, https://bioweb.bio), and *G. seraphini* (© Brian Freiermuth, with permission).

3.3.4 Synteny analyses. We investigated synteny among genes near *LWS* in the three available caecilian genomes and compared them to other available amphibian genomes. Consistent with the findings of Lin et al. (2024), we found that the syntenic block containing *HCFC1*, *TMEM187*, *IRAK1*, *MECP2*, *SWS2*, and *LWS* is conserved among amphibians. However, the three caecilian genomes are missing *SWS2*. which may have been lost in the ancestor of Gymnophiona (Figure 1; Supplementary Data 4).

3.3 SELECTION ANALYSES

Results from the complete and incomplete *LWS* analyses were congruent (Supplementary Material File 1 and 2). Thus, we only present the complete dataset. Results from the incomplete dataset are provided in Supplementary Material Section 3.

We found that the M3 model was a better fit than M0 for both genes (*RH1*: likelihood ratio (LR) = 615.675, P = 0.0000; *LWS*: LR = 825.605, P = 0.0000; File S2), suggesting significant ω variation across sites. Additionally, to test for positively selected sites, we compared the fit of the M8 model, which allows for sites with $\omega > 1$, to that of M7 and M8a. For *RH1*, the M8 model was a better fit than M7 (LR = 40.181, P = 0.0000; File S2) and M8a (LR = 5.978, P = 0.015; File S2). Two sites were inferred to be under positive selection with a BEB

posterior probability >90% (positions 213 and 217; bovine *RH1* numbering), while one site did was close to but did not meet the significance threshold (position 107). Consistently, BUSTED found nearly significant evidence for gene-wide episodic diversifying selection of *RH1* in caecilians (P = 0.059) and identified two sites with evidence ratios (ER) ≥ 100 (positions 107 and 213), aligning with CODEML.

In contrast, for *LWS*, M8 was a better fit than M7 (LR = 44.241, P < 0.00001; File S2) but not M8a (LR = 0.0, P = 1.0; File S2), indicating only a weak signal for positive selection. Only one site exceeded the 90% BEB significance threshold (site 66; 49 in bovine *RH1*). Meanwhile, BUSTED did not detect gene-wide episodic diversifying selection in caecilian *LWS* sequences (P = 0.081) and found no sites under positive selection.

The FEL and FUBAR analyses can detect signals of positively selected sites across the entire phylogeny. However, FUBAR did not identify any sites for *LWS* or *RH1*. On the other hand, FEL identified one site under diversifying positive selection in *LWS* when the stem caecilian clade was used as foreground (site 109; 92 in bovine *RH1;* P = 0.04), but not across the entire phylogeny. In contrast, for *RH1*, FEL identified one site under positive selection across the entire phylogeny (119; P = 0.05) and a different site when the stem caecilian clade was analyzed as foreground (292; P = 0.04). Interestingly, FEL results showed that 272 out of 368 codon sites (when no foreground was identified) and 175 out of 368 codon sites (when caecilians were defined as the test group) in *LWS* were under purifying selection at p ≤ 0.05. This pattern of purifying selection is similar to that observed in the functional *RH1*, where 247 out of 354 codon sites (no foreground) and 165 out of 354 codon sites (caecilians foreground) were under purifying selection at the same significance threshold.

These findings suggest that selection is acting to preserve the integrity of visual opsin gene sequences and maintain their function over evolutionary time.

Our analysis using RELAX revealed an overall relaxation of selective constraint in *LWS* but not *RH1* when crown Gymnophiona and its stem branch were designated as the foreground (*LWS:* K = 0.74, LR = 15.47, P = 0.000; *RH1*: K = 1.37, LR = 1.67, P = 0.196; Figure 1C and File S2). This pattern was further supported by CODEML. Specifically, both clade model C (CmC vs M2a_rel: LRT = 8.507, P = 0.004) and clade model D (CmD vs. M3: LRT = 11.055, P = 0.0009) were supported over other models, providing significant evidence for shifts in selection pressures, with some sites in *LWS* showing a transition from relatively stronger to weaker purifying selection within Gymnophiona + stem. For *RH1*, however, neither the CmC nor CmD models were favored over the alternative models (CmC vs M2a_rel: LRT = 0.508, P = 0.476; CmD vs M3: LRT = 3.053, P = 0.08), suggesting that selective pressure on *RH1* has not undergone significant evolutionary shifts in caecilians (File S2).

3.4 CAECILIAN RETINAL MORPHOLOGY

280 microphotographs of retinae representing 8 of the 10 families of Gymnophiona were examined (see Supplementary Material Table 2 for specimen information). All specimens examined had well organized retinae containing all the cellular layers typical for visual vertebrates with the possible exception of *Scolecomorphus uluguruensis*, but this may be due to preservation artifacts (see Figure 4F). Sections with well preserved retinal morphology were selected to highlight retinal diversity across Gymnophiona (Figures 3 and 4; Table 2).

Epicrionops sp. (Figure 3A). Rods cylindrical, outer segments similar thickness to inner segments. Outer nuclear layer (ONL) 2–3 rows tightly packed spherical nuclei. Inner nuclear layer (INL) 3–4 rows loosely packed spherical nuclei, ~40 µm. Outer plexiform layer (OPL) inconspicuous due to loosely packed nuclei in INL. Ganglion cell layer (GCL) 1–2 nuclei deep. Lens ellipsoid. Two cone-like photoreceptors highlighted in Figures 4A and 4B.

Ichthyophis kohtaoensis Retina distorted, compressed so lens contacts retina. Rod outer segments shorter in medial retina, longer near retinal margin. Rod outer segment size variability may be due to section distortion; however, similar pattern seen by Himstedt (1995). Rods cylindrical, outer segment thickness similar to inner segments. ONL 1–2 rows tightly packed ellipsoid nuclei. INL 2–3 rows tightly packed spherical nuclei. Lens ellipsoid. Cone-like photoreceptor indicated in Figure 4C.

Dermophis mexicanus Rod outer segments thinner at base than inner segments, tapering slightly distally (may be due to stretching of the rods). ONL 2–3 rows of tightly packed spherical nuclei. INL 3–4 rows loosely packed spherical nuclei; ~62 µm. Boundary between ONL and INL not clearly defined, so OPL inconspicuous. GCL 2–3 nuclei thick. Lens ellipsoid. Cone-like photoreceptor indicated in Figure 4D. Figure 4F shows photoreceptor tendency to be stretched, peel from pigment epithelium (PE), a common preservation artifact in retinal sections.

Typhlonectes compressicauda Retina cracked, compressed/shrunken; maintains general shape. Individual photoreceptor morphology not discernible. External limiting membrane (ELM) to PE ~5 µm. ONL 1–2 rows tightly packed ellipsoid or irregularly shaped nuclei; ~20µm. INL 3–4 rows packed nuclei; 25–28 µm. OPL not clearly defined, < 3 µm where visible. GCL 1–2 rows nuclei. Lens spherical.

Scolecomorphus kirkii Rods columnar; outer segments slightly thinner than inner segments, without narrowing at end. ONL 2–3 rows of packed spherical nuclei. INL 2–3 rows moderately packed spherical nuclei, 20–28 µm (smaller near the retinal margin). GCL one nucleus deep; nuclei not contiguous layer throughout length. Lens amorphous, contiguous to GCL. In Figure 4E, a cone-like photoreceptor indicated with black arrow; photoreceptor similar to double rod indicated with blue arrow.

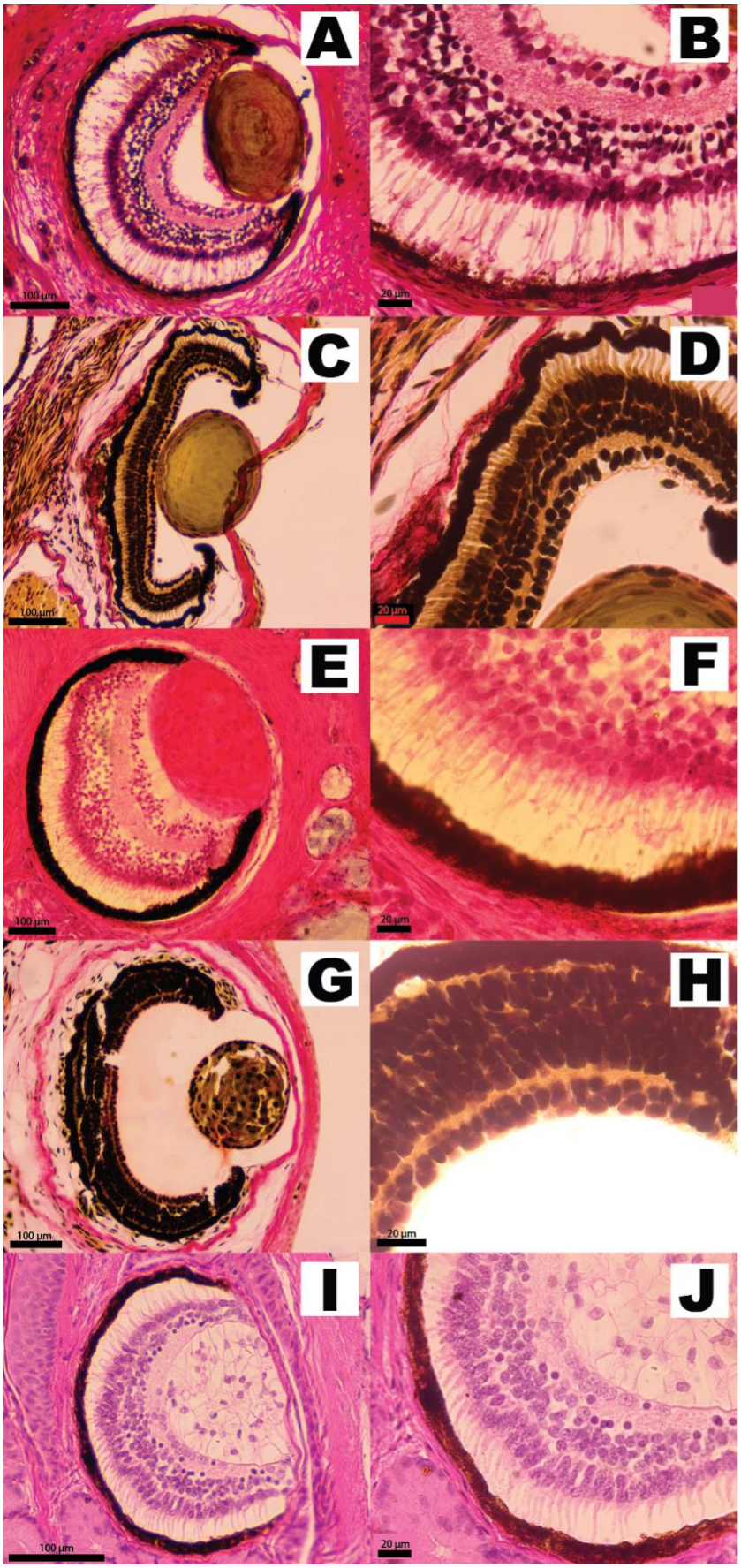
A
B
C
D
E
F
G
H
I
J
100 µm
20 µm
100 µm
20 µm
100 µm
20 µm
100 µm
20 µm
100 µm
20 µm

FIGURE 3. A selection of photomicrographs and schematic drawings of retinae from five species of caecilians at 100X and 400X magnification. (A, B) *Epicrionops sp.* (S-book 367b, slide 98; Sagittal, Picro-Ponceau). (C, D) *Ichthyophis kohtaoensis* (S-book 448b, slide 11; Frontal, Picro-Ponceau). (E, F) *Dermophis mexicanus* (S-book 162, slide 8; Frontal, Mallory's Azan). (G, H) *Typhlonectes compressicauda* (S-book 241, slide 20; Frontal, Picro-Ponceau). (I, J) *Scolecomorphus kirkii* (S-book 230R, slide 19; Frontal, Hematoxylin and Eosin).

Table 2. Summary of characters reported from sections shown in Figure 3.

Species	**Inner Rod Segment Length (µm)**	**Outer Rod Segment Length (µm)**	**Outer Plexiform Layer width (µm)**	**Inner Plexiform Layer width (µm)**	**Number of nuclei rows in ONL**	**Number of nuclei rows in INL**	**Number of nuclei rows in GCL**	**Lens Shape**
Epicrionops sp.	10	35–40	NA	40	2–3	3–4	1–2	ellipsoid
Ichthyophis kohtaoensis	5	8–14	2–4	7–10	1–2	2–3	1–2	ellipsoid
Dermophis mexicanus	10	30–35	NA	46	2–3	3–4	2–3	ellipsoid
Typhlonectes compressicauda	N/A (see text)	N/A (see text)	< 3	5–8	1–2	3–4	1-2	spherical

Scolecomorphus kirkii	8	15–20	2–5	12	2–3	2–3	1, discontiguous	amorphous

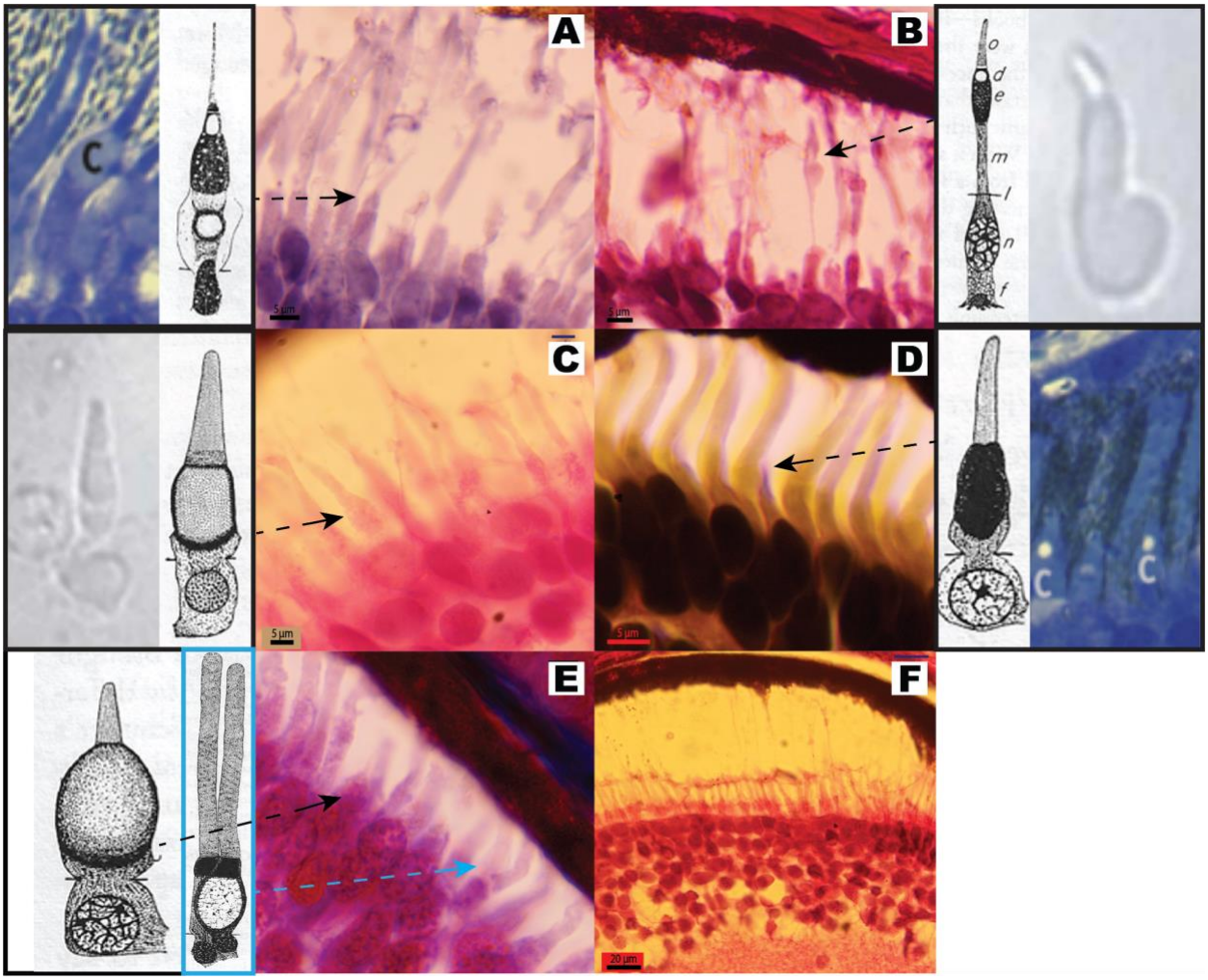

FIGURE 4. A selection of photomicrographs demonstrating photoreceptor cell diversity in Gymnophiona. Black arrows point to photoreceptors that exhibit characteristics typical of cone photoreceptors (bulbous ellipsoids, tapered outer segments that are much thinner than their inner segments) while the blue arrow indicates a photoreceptor reminiscent of a double rod. These are

morphologically distinct from the rods that predominate the caecilian retina. Alongside each panel, we include diagrams and images of cone photoreceptors and one double rod diagram that resemble the structures we identified. (A) *Epicrionops sp.* (S-book 367b, slide 97; Sagittal, Hematoxylin-Eosin). (B) *Epicrionops sp.* (S-book 367b, slide 98; Sagittal, Picro-Ponceau). (C) *Dermophis mexicanus* (S-book 162, slide 8; Frontal, Mallory's Azan). (D) *Ichthyophis kohtaoensis* (S-book 448b, slide 11; Frontal, Picro-Ponceau). (E) *Scolecomorphus kirkii* (S-book 230L, slide 30; Frontal, Mallory's Azan). (F) *Dermophis mexicanus* (S-book 162, slide 9; Frontal, Mallory's Azan). This image demonstrates the tendency of photoreceptors to become stretched and peel off of the pigment epithelium (PE) due to separation of the PE from the photoreceptor layer, a common preservation artifact in retinal sections. All images were taken at 1000X magnification except for (F) which was taken at 400X magnification. The drawings are sourced from (Walls, 1942). The blue diagrams were adapted from "A frog's eye view: Foundational revelations and future promises", Vol. 106, Donner and Yovanovich, Page No. 74, Copyright © 2020, with redistribution license 926070910619 from Elsevier. The grey images were adapted from "Co-expression of three opsins in cone photoreceptors of the salamander, *Ambystoma tigrinum*", Vol 522, Isayama et al. Page No. 21, Copyright © 2013 Wiley Periodicals, Inc. with redistribution license 5926071480344. Letter abbreviations for the diagram associated with (B) are as follows: o - outer segment; d - oil droplet; e - ellipsoid; m - myoid; l - external limiting membrane; n - nucleus; f - foot-piece.

3.5 ANCESTRAL CHARACTER STATE RECONSTRUCTION

Ancestral character reconstruction of eye musculature shows that the ancestral condition was the presence of all six eye muscles (Figure 5A). The most highly supported scenario appears to involve a reduction to two muscles followed by two independent gains of all muscles, one in *Dermophis* and another in *Hypogeophis*. Reconstruction of eye exposure shows that the ancestral condition for Gymnophiona is eye covered by skin (Figure 5B). From that ancestral condition, there have been four independent gains of eye covered by bone in *Boulengerula*, *Caecilia gracilis*, *Oscaecilia* and in *Gymnopis*. Note that the character is labile in the caecilids *C. gracilis* and *O. ochrocephala* (See Supplementary Material Section 4.1).

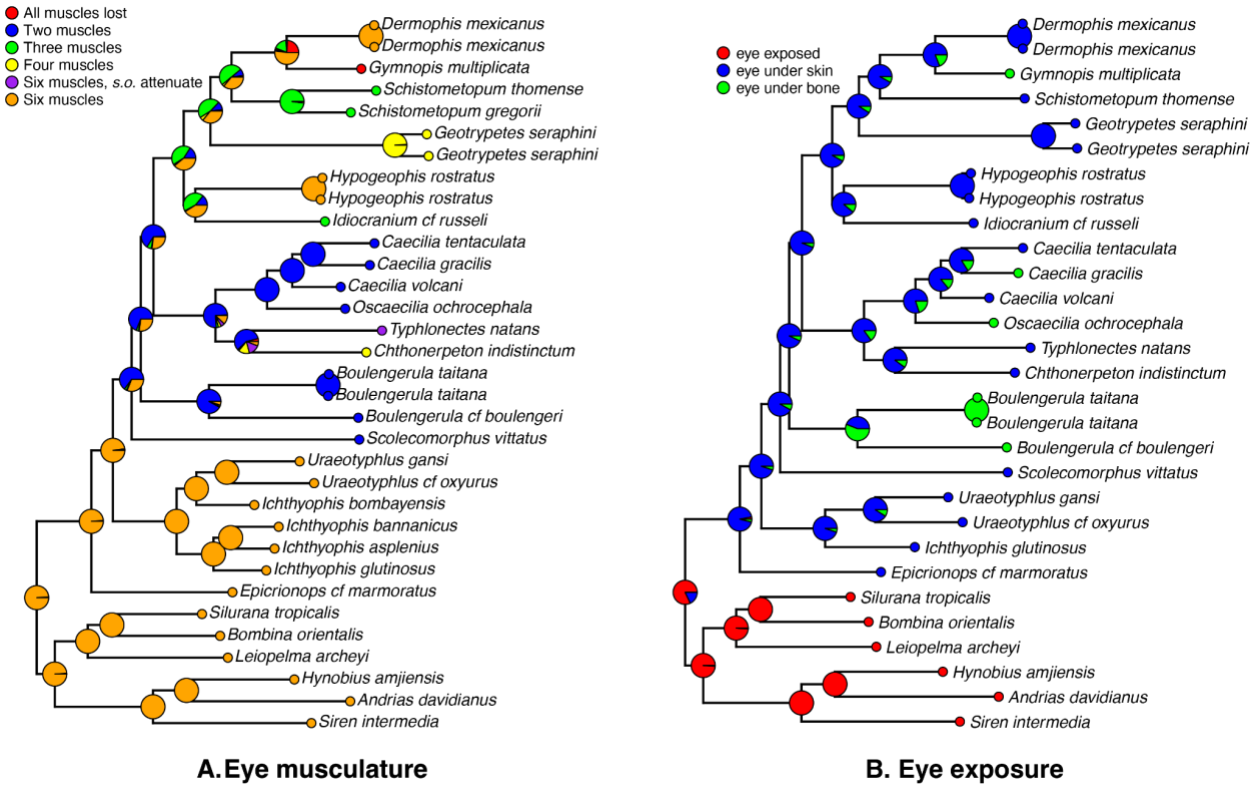

FIGURE 5. Posterior probabilities at each ancestral node for eye exposure and eye musculature condition. Probabilities were obtained from stochastic character mapping using model weights to sample three (A) or two (B) different Mk trait evolution models. See text for details.

4. DISCUSSION

4.1. Expression of* LWS *and morphology of caecilian retinae. For such a unique and ancient vertebrate order, caecilians are woefully understudied, and their genomes are no exception (Torres-Sánchez et al., 2019). Prior to work by Lin et al. (2024), caecilian eyes were thought to have rod-based retinae that only contain rhodopsin (Mohun et al., 2010; Wake, 1985). Here we report putatively functional *LWS* sequences from an additional five caecilian families, covering eight of the ten families in Order Gymnophiona, and indicating that *LWS* was most likely present in the most recent common ancestor of all caecilians.

Given that these *LWS* sequences have a translatable open reading frame and a stop codon position homologous to other amphibian *LWS* sequences (Supplementary Material Data 2), and that the gene is expressed in the eye of at least one caecilian species (Figure 1B), we hypothesize that *LWS* is functionally expressed and under purifying selection in caecilian eyes. Our *LWS* expression data comes from *Caecilia orientalis*, a member of Caeciliidae known for derived fossorial adaptations and relatively reduced eyes (Wake, 1985). These results indicate that *LWS* expression in this species is significantly lower than *RH1*, aligning with observations in the frog *Rana sphenocephala*, where adult individuals express *RH1* at about 50 times the level of *LWS* (Schott et al., 2022). Similarly, in some dim-light adapted (e.g., deep-water, nocturnal) fish species, *LWS* expression relative to *RH1* can be very low (Fogg et al., 2022; Luehrmann et al., 2019). However, some diurnal species also show relatively low *LWS* expression, such as the spotted unicorn fish (*Naso brevirostris*) (Tettamanti et al., 2019). The relatively low expression

of *LWS* may be a result of a rod-biased (or rod-only) retina, a pattern which is not unique to but is often prominent in nocturnal species. The common ancestor of Amphibia was likely nocturnal (Anderson & Wiens, 2017), and salamanders and anurans possess a higher proportion of rods to cones in their retinae (Donner & Yovanovich, 2020; Fain, 1976; Nilsson, 1964; Walls, 1942).

Existing literature and our morphological review of caecilian retinae do not provide conclusive support for the presence of cone cells in any caecilian species. Cone cells could be overlooked if they are inconspicuous and highly outnumbered by large rod cells, which is consistent with our 80:1 *RH1* to *LWS* mRNA transcript ratio. Thus, observations of photoreceptors with cone-like characteristics could be dismissed as anomalous variation, damaged cells, or rod outer segments in a state of regeneration. We carefully inspected over 280 images in order to encounter the handful of putative cone-like cells. There is considerable morphological variation among these cone-like photoreceptors, and, given the extreme variation in cone morphology observed among vertebrates (even at relatively young evolutionary time scales, e.g., in colubrid snakes; Walls, 1942), it is impossible to know what caecilian cones might look like and how similar or different they are among families, some of which likely diverged nearly 200 MYA (Kligman et al., 2023). We acknowledge that given the distortions and artifacts observed in retinal sections, the cone-like photoreceptors we highlighted may be rod cells with anomalous or misleading morphologies as described above.

It is plausible that *LWS* is expressed in rod cells. For example, the cone opsin *SWS2* is expressed in ‘green rods’ of frogs and salamanders (W. I. L. Davies et al., 2012), which, in conjunction with ‘red rods’ expressing *RH1,* is thought to aid in nocturnal color vision (Yovanovich et al., 2017). Additionally, Gower et al. (2021) found that *LWS* was co-expressed with *RH1* in rod cells of *Anilios bicolor,* a fossorial scolecophidian snake with highly reduced

eyes. Thus, a similar phenomenon could be occurring in caecilians. Immunolabeling studies employing antibodies against *LWS* or other proteins specific to cones and the cone phototransduction pathway will be necessary to confirm their presence in the caecilian retina.

As far as we are aware, our study presents the first set of eye transcriptome data for any caecilian, so we are not certain if the two transcripts that we identified are artifacts of the assembly process or represent alternatively spliced transcripts. The genome assemblies of *R. bivittatum*, *M. unicolor*, and *G. seraphini* only contain one annotated transcript, but as far as we are aware, the assembly process did not incorporate eye transcriptome data (Ovchinnikov et al., 2023). Moreover, neither our transcriptomic analysis nor our genome mining approaches, including the synteny analysis by Lin et al (2024), were able to detect the cone opsin genes *SWS1* and *SWS2*. These genes are believed to have been present in Lissamphibia and are known from the other two extant orders of amphibians, Urodela (newts and salamanders) and Anura (frogs) (W. L. Davies, 2011).

4.2. Functional implications and ecological persistence of* LWS *in caecilians. When analyzing the amino acid composition of known spectral tuning sites in available *LWS* and *RH1* sequences for caecilians, we found that they are consistent with data reported for other amphibians (Schott et al., 2024; Wan et al., 2023), containing at least one of the known amino acid variants at each site (see Supplementary Material Table 6). For example, as highlighted by Lin et al. (2024), the specific combination of S164, H181, Y261, T269, and A292 found in the *LWS* sequence of *R. bivitatum*, *G. seraphini*, *M. unicilor*, and *C. orientalis* has been shown to generate a long-wavelength-sensitive photopigment with λ_{max} at ~560 nm in other vertebrates (Asenjo et al., 1994; Hauzman et al., 2017; Yokoyama, 2002; Yokoyama & Radlwimmer, 2001). While this prediction is relatively close to our machine learning estimates (546.87–550.58 nm;

excluding *C. orientalis LWS_v2*), our estimates fall on the shorter end of the range observed in the vertebrate *LWS* ((~549–626 nm; Schott et al., 2024)), similar to the absorbance properties observed in nocturnal terrestrial species (Margetts et al., 2024; Veilleux & Cummings, 2012). If accurate, these short absorbance values could enhance low-light vision by improving the signal-to-noise ratio through reduced thermal noise susceptibility (Luo et al., 2011).

It is important to note, however, that our machine learning (ML) model showed only a weak correlation with MSP data for *LWS* (r = 0.13, P = 0.66), possibly because of an underrepresentation of opsins in the ~600-nm range within the ML training dataset (Frazer et al., 2024). Additionally, variation in MSP data cannot be ruled out; for instance, *Ambystoma tigrinum* show a 30–40 nm range in MSP data for red cones (Makino & Dodd, 1996). This variation likely stems from the challenges of estimating absorbance in single cone photoreceptors, especially for *LWS* in amphibians, as it is more susceptible to noise and generally has smaller sample sizes compared to rod pigments like *RH1* or *SWS2* (see Supplementary material in Schott et al., 2024).

LWS is present in a significant proportion of fossorial and low-light adapted taxa, such as blind mole rats, cryptozooic Australian scincid lizards, and some deep-sea fish species (W. I. L. Davies et al., 2012; Ford et al., 2024; Musilova et al., 2021). Most reported instances of *LWS* gene loss or pseudogenization occur in fishes adapted to deep sea environments (Lin et al., 2017; Musilova et al., 2021), where light in the long wavelength end of the visual spectrum is minimal or absent. To our knowledge, pseudogenization of *LWS* in tetrapods has only been observed in the subterranean naked mole-rat (*Heterocephalus glaber*), the Cape golden mole (*Chrysochloris asiatica*) and deep diving whales (Emerling & Springer, 2014; Meredith et al., 2013). Dysfunction or complete loss of *LWS* is possible in the obligate subterranean Texas blind

salamander (*E. rathbuni*), given that Tovar et al. (2021) were unable to label any of the visual opsins in the retina. However, failure to immunochemically label LWS in the retina is not necessarily confirmation of gene loss or dysfunction. For example, in one population of the blind cave salamander (*Proteus anguinus anguinus*), Kos et al. (2001) found the LWS protein in the pineal gland but not the eye, while both tissues from other populations were successfully immunolabeled for LWS (Kos et al., 2001). These data show that the *LWS* gene tends to persist in ecological and evolutionary contexts under which other cone opsins are readily lost, strongly suggesting that *LWS* retains some function even in species with highly reduced visual systems.

Additional evidence for the potential functionality of *LWS* in caecilians arises from our selection analyses. With the shift to a fossorial lifestyle, caecilians underwent a simplification of their visual systems, likely leading to relaxed selection on the molecular mechanisms underlying vision, and eventually to the loss of some cone opsins. While the loss of *SWS1* and *SWS2* (Lin et al., 2024; Mohun et al., 2010) might be the result of relaxed selection, the same selective environment did not result in the loss of *LWS*, although the signal of relaxation remains detectable in caecilian *LWS* sequences (see Results section 3.3). Importantly, this relaxation in selective pressure did not result in an overabundance of deleterious mutations, as the *LWS* sequences retrieved from caecilian genomes and transcriptome have intact open reading frames. Given this long-term retention of *LWS* (over 240 million years; Kligman et al., 2023), we hypothesize that some degree of purifying selection has preserved its functionality, despite the relaxed constraints associated with reduced visual demands. A similar pattern is observed in bats, where relaxed selection on *LWS* in echolocating species has not led to its loss or pseudogenization over tens of millions of years, suggesting a potential role beyond vision (Wertheim et al., 2015).

One possible function for *LWS* could be tied to behavioral ecology. Light between 520 and 610 nm is most prominent in the forest understory while in more open woodland environments wavelengths below 500 nm are more prevalent (Endler, 1993). Thus, slight variations in blue to red wavelengths may provide caecilians information about canopy cover, habitat type, and exposure to predators when they are at or near the surface in forested habitats. Furthermore, there are significant shifts in light intensity within forests at long and short wavelengths in the transition from daylight, to sunset, to twilight (Endler, 1993). Dichromatic vision is possible with only rods (*RH1*) and red cones (*LWS*) under mesopic conditions (W. I. L. Davies et al., 2012; Hunt et al., 2009) and could afford caecilians the spectral resolution necessary to discriminate between these structural and temporal variables of their environment. As caecilians appear to be primarily nocturnal (Prakash et al., 2024) and most observations of surface activity occur at night or twilight, distinguishing blue from yellow/orange light may be important for informing activity patterns and entraining circadian rhythm. *LWS* may also provide some visual information when caecilians find themselves at the surface under bright daylight conditions that would render rods useless due to saturation. Light intensity and spectra may be the only visual information available to caecilians. Therefore, retaining some spectral discrimination may allow them to maximize the visual information available given the constraints imposed by adaptation for head-first burrowing.

4.4. Evolution of caecilian eyes. Caecilians (Gymnophiona) are an ancient order of amphibians whose ancestor began transitioning to a fossorial lifestyle more than 190 million years ago (Kligman et al., 2023; Santos et al., 2020). Caecilians have undergone a degeneration of visual organs associated with an increasingly fossorial lifestyle (Himstedt, 1995; Kamei et al., 2012; Taylor, 1968), including losing two of three cone opsin genes (Lin et al., 2024; this study;

Mohun et al., 2010; Musser & Arendt, 2017). Patterns in trait loss are not necessarily correlated with species ecology or phylogeny. For example, *Dermophis mexicanus* and *Gymnopis multiplicata* are closely related and ecologically similar members of Dermophiidae from Central America: they are viviparous, live as litter burrowers in shallow soil, and emerge at dawn and dusk, especially in light rains, to forage (MHW pers. obs.). *Dermophis mexicanus* have relatively well-developed eyes in open sockets, covered by skin, with all six extrinsic muscles, a cell-rich, organized retina, and a crystalline lens that retains some cells peripherally. In contrast, *Gymnopis multiplicata* has eyes in sockets covered by bone as well as skin, no extrinsic muscles, a cell-poor and disorganized retina, and an amorphous cellular lens that is usually flattened against the cornea and retina (Wake, 1985). In another example, the covering of the eye socket by bone is a homoplastic character that occurs in members of several families: Caeciliidae (*Oscaecilia* and *Caecilia*), Dermophiidae (*Gymnopis*, *Dermophis*), Herpelidae (*Boulengerula*), and Scolecomorphidae (*Scolecomorphus*, *Crotaphatrema*). *Scolecomorphus* has an exceptional morphology: the eyes in at least three species are not in the sockets but embedded in the tentacle (De Jager, 1940; Taylor, 1968; Wake, 1985). It is tempting to consider the covered eye as a factor driving further degeneration of the visual apparatus in these taxa (Wake, 1985), yet the morphological patterns are not exactly similar, with different elements being more reduced or lost among the species in the set, including among *Scolecomorphus* species. These examples illustrate the mosaic loss of visual features across the history of caecilians, likely as a result of the relaxed selection that appears to be a feature of the clade.

5. CONCLUSION

Although previous work suggested that the loss of *LWS* may be a synapomorphy of caecilians, we find that caecilians possess the *LWS* gene. Yet, the function of this opsin is unknown. Across caecilians, the gene appears to be under relaxed selection, which suggests a change in function. Although we find that *LWS* is expressed in the eye of one caecilian species, we cannot say whether it is translated into a protein. The maintenance of the open reading frame, however, suggests some function of the mRNA, and/or of the protein, if it exists. We propose that *LWS* may function to transmit light signals to other genes that regulate activity patterns (Boyette et al., 2024) or that it is used to complement wavelength or luminance information obtained with *RH1* under mesopic conditions. Although traits are almost never completely lost (Sadier et al., 2022), it is interesting that *LWS*, which is a terminal gene in the visual cascade, is maintained for such a long time under fossorial conditions. The maintenance of *LWS* in caecilians and other dim-light-adapted animals begs the question of what this opsin does and why it is still useful – i.e., why *LWS* and not the other opsins? These data pose new questions regarding the pressures associated with dim-light or fossorial lifestyles, the biology of caecilians, including the presence of bright coloration and above-ground behavior in some species, as well as an interesting example of the mosaic nature of trait loss.

References

Anderson, S. R., & Wiens, J. J. (2017). Out of the dark: 350 million years of conservatism and evolution in diel activity patterns in vertebrates. *Evolution*, 71(8), 1944–1959.

Andrews, S. (2010). *FastQC: a quality control tool for high throughput sequence data*.

Asenjo, A. B., Rim, J., & Oprian, D. D. (1994). Molecular determinants of human red/green color discrimination. *Neuron*, 12(5), 1131–1138.

Bielawski, J. P., & Yang, Z. (2004). A maximum likelihood method for detecting functional divergence at individual codon sites, with application to gene family evolution. *Journal of Molecular Evolution*, 59(1), 121–132.

Bowmaker, J. K. (2008). Evolution of vertebrate visual pigments. *Vision Research*, 48(20), 2022–2041.

Boyette, J. L., Bell, R. C., Fujita, M. K., Thomas, K. N., Streicher, J. W., Gower, D. J., & Schott, R. K. (2024). Diversity and molecular evolution of nonvisual opsin genes across environmental, developmental, and morphological adaptations in frogs. *Molecular Biology and Evolution*, 41(6).

Carmona, F. D., Glösmann, M., Ou, J., Jiménez, R., & Collinson, J. M. (2009). Retinal development and function in a "blind" mole. *Proceedings of the Royal Society B: Biological Sciences*, 277(1687), 1513–1522.

Carmona, F. D., Ou, J., Jiménez, R., & Collinson, J. M. (2010). Development of the cornea of true moles (Talpidae): morphogenesis and expression of PAX6 and cytokeratins. *Journal of Anatomy*, 217(5), 488–500.

Catania, K. C. (1999). A nose that looks like a hand and acts like an eye: the unusual mechanosensory system of the star-nosed mole. *Journal of Comparative Physiology. A, Sensory, Neural, and Behavioral Physiology*, 185(4), 367–372.

Chen, Y.-A., Lin, C.-C., Wang, C.-D., Wu, H.-B., & Hwang, P.-I. (2007). An optimized procedure greatly improves EST vector contamination removal. *BMC Genomics*, 8(1), 416.

Chernomor, O., von Haeseler, A., & Minh, B. Q. (2016). Terrace Aware Data Structure for Phylogenomic Inference from Supermatrices. *Systematic Biology*, 65(6), 997–1008.

Davies, W. I. L., Collin, S. P., & Hunt, D. M. (2012). Molecular ecology and adaptation of visual

photopigments in craniates. *Molecular Ecology*, 21(13), 3121–3158.

Davies, W. L. (2011). Adaptive gene loss in vertebrates: Photosensitivity as a model case. In *Encyclopedia of Life Sciences*. John Wiley & Sons, Ltd.

De Jager, E. F. J. (1940). *Cranial Morphology of the Gymnophiona*. University of Stellenbosch.

Delport, W., Poon, A. F. Y., Frost, S. D. W., & Kosakovsky Pond, S. L. (2010). Datamonkey 2010: a suite of phylogenetic analysis tools for evolutionary biology. *Bioinformatics* , 26(19), 2455–2457.

Donner, K., & Yovanovich, C. A. M. (2020). A frog's eye view: Foundational revelations and future promises. *Seminars in Cell & Developmental Biology*, 106, 72–85.

Dünker, N. (1998). Colocalization of serotonin and GABA in retinal neurons of *Ichthyophis kohtaoensis* (Amphibia; Gymnophiona). *Anatomy and Embryology*, 197(1), 69–75.

Edgar, R. C. (2004). MUSCLE: multiple sequence alignment with high accuracy and high throughput. *Nucleic Acids Research*, 32(5), 1792–1797.

Emam, A., Yoffe, M., Cardona, H., & Soares, D. (2020). Retinal morphology in *Astyanax mexicanus* during eye degeneration. *The Journal of Comparative Neurology*, 528(9), 1523–1534.

Emerling, C. A., & Springer, M. S. (2014). Eyes underground: regression of visual protein networks in subterranean mammals. *Molecular Phylogenetics and Evolution*, 78, 260–270.

Emerson, S. B. (1976). Burrowing in frogs. *Journal of Morphology*, 149(4), 437–458.

Endler, J. A. (1993). The color of light in forests and its implications. *Ecological Monographs*, 63(1), 1–27.

Espinasa, L., & Jeffery, W. R. (2006). Conservation of retinal circadian rhythms during cavefish eye degeneration. *Evolution & Development*, 8(1), 16–22.

Fain, G. L. (1976). Sensitivity of toad rods: Dependence on wave-length and background illumination. *The Journal of Physiology*, *261*(1), 71–101.

Fogg, L. G., Cortesi, F., Lecchini, D., Gache, C., Marshall, N. J., & de Busserolles, F. (2022). Development of dim-light vision in the nocturnal reef fish family Holocentridae. I: Retinal gene expression. *The Journal of Experimental Biology*, 225(17), jeb244513.

Ford, M. J. R., Ludington, A. J., Bradford, T., Sanders, K. L., Hutchinson, M. N., & Simões, B. F. (2024). Retention of the full visual opsin repertoire in Australia's cryptozoic lizards. In *bioRxiv* (p. 2024.02.19.581082).

Foureaux, G., Egami, M. I., Jared, C., Antoniazzi, M. M., Gutierre, R. C., & Smith, R. L. (2010). Rudimentary eyes of squamate fossorial reptiles (amphisbaenia and serpentes). *Anatomical Record (Hoboken, N.J.: 2007)*, 293(2), 351–357.

Frazer, S. A., Baghbanzadeh, M., Rahnavard, A., Crandall, K. A., & Oakley, T. H. (2024). Discovering genotype-phenotype relationships with machine learning and the Visual Physiology Opsin Database (VPOD). In *bioRxiv* (p. 2024.02.12.579993).

Glösmann, M., Steiner, M., Peichl, L., & Ahnelt, P. K. (2008). Cone photoreceptors and potential UV vision in a subterranean insectivore, the European mole. *Journal of Vision*, 8(4):23, 1–12.

Gower, D. J., Fleming, J. F., Pisani, D., Vonk, F. J., Kerkkamp, H. M. I., Peichl, L., Meimann, S., Casewell, N. R., Henkel, C. V., Richardson, M. K., Sanders, K. L., & Simões, B. F. (2021). Eye-transcriptome and genome-wide sequencing for Scolecophidia: Implications for inferring the visual system of the ancestral snake. *Genome Biology and Evolution*, 13(12).

Grabherr, M. G., Haas, B. J., Yassour, M., Levin, J. Z., Thompson, D. A., Amit, I., Adiconis, X., Fan, L., Raychowdhury, R., Zeng, Q., Chen, Z., Mauceli, E., Hacohen, N., Gnirke, A.,

Rhind, N., di Palma, F., Birren, B. W., Nusbaum, C., Lindblad-Toh, K., … Regev, A. (2011). Full-length transcriptome assembly from RNA-Seq data without a reference genome. *Nature Biotechnology*, 29(7), 644–652.

Haas, B. J. (n.d.). *TransDecoder*. TransDecoder v2.026. Retrieved 2021, from https://github.com/TransDecoder/TransDecoder

Haussler, D., O'Brien, S. J., Ryder, O. A., Keith Barker, F., Clamp, M., Crawford, A. J., Hanner, R., Hanotte, O., Johnson, W. E., McGuire, J. A., Miller, W., Murphy, R. W., Murphy, W. J., Sheldon, F. H., Sinervo, B., Venkatesh, B., Wiley, E. O., Allendorf, F. W., Amato, G., … Turner, S. (2009). Genome 10K: A Proposal to Obtain Whole-Genome Sequence for 10 000 Vertebrate Species. *The Journal of Heredity*, 100(6), 659–674.

Hauzman, E., Bonci, D. M. O., Suárez-Villota, E. Y., Neitz, M., & Ventura, D. F. (2017). Daily activity patterns influence retinal morphology, signatures of selection, and spectral tuning of opsin genes in colubrid snakes. *BMC Evolutionary Biology*, 17(1), 249.

Himstedt, W. (1995). Structure and function of the eyes in the caecilian *Ichthyophis kohtaoensis* (Amphibia, Gymnophiona). *Zoology-Analysis of Complex Systems*, 99(1), 81–94.

Holmberg, B. J. (2022). Ophthalmology of Eulipotyphla: Moles, Shrews, Hedgehogs, and Relatives. In F. Montiani-Ferreira, B. A. Moore, & G. Ben-Shlomo (Eds.), *Wild and Exotic Animal Ophthalmology: Volume 2: Mammals* (pp. 355–366). Springer International Publishing.

Humason, G. L. (1979). *Animal Tissue Techniques*. W. H. Freeman.

Hunt, D., Carvalho, L. S., Cowing, J. A., & Davies, W. L. (2009). Evolution and spectral tuning of visual pigments in birds and mammals. *Philosophical Transactions of the Royal Society of London. Series B, Biological Sciences*, 364(1531), 2941–2955.

Jenkins, P. a., & Walsh, D. M. (1993). An Early Jurassic caecilian with limbs. *Nature*, 365, 246–250.

Jetz, W., & Pyron, R. A. (2018). The interplay of past diversification and evolutionary isolation with present imperilment across the amphibian tree of life. *Nature Ecology & Evolution*, 2(5), 850–858.

Jones, P., Binns, D., Chang, H.-Y., Fraser, M., Li, W., McAnulla, C., McWilliam, H., Maslen, J., Mitchell, A., Nuka, G., Pesseat, S., Quinn, A. F., Sangrador-Vegas, A., Scheremetjew, M., Yong, S.-Y., Lopez, R., & Hunter, S. (2014). InterProScan 5: genome-scale protein function classification. *Bioinformatics (Oxford, England)*, 30(9), 1236–1240.

Kalyaanamoorthy, S., Minh, B. Q., Wong, T. K. F., von Haeseler, A., & Jermiin, L. S. (2017). ModelFinder: fast model selection for accurate phylogenetic estimates. *Nature Methods*, 14(6), 587–589.

Kamei, R. G., Mauro, D. S., Gower, D. J., Van Bocxlaer, I., Sherratt, E., Thomas, A., Babu, S., Bossuyt, F., Wilkinson, M., & Biju, S. D. (2012). Discovery of a new family of amphibians from northeast India with ancient links to Africa. *Proceedings of the Royal Society B: Biological Sciences*, 279, 2396–2401.

Katoh, K., & Standley, D. M. (2013). MAFFT multiple sequence alignment software version 7: improvements in performance and usability. *Molecular Biology and Evolution*, 30(4), 772–780.

Kligman, B. T., Gee, B. M., Marsh, A. D., Nesbitt, S. J., Smith, M. E., Parker, W. G., & Stocker, M. R. (2023). Triassic stem caecilian supports dissorophoid origin of living amphibians. *Nature*, 614(7946), 102–107.

Kosakovsky Pond, S. L., & Frost, S. D. W. (2005). Not so different after all: a comparison of

methods for detecting amino acid sites under selection. *Molecular Biology and Evolution*, 22(5), 1208–1222.

Kos, M., Bulog, B., Szél, A., & Röhlich, P. (2001). Immunocytochemical demonstration of visual pigments in the degenerate retinal and pineal photoreceptors of the blind cave salamander (Proteus anguinus). *Cell and Tissue Research*, 303(1), 15–25.

Kumar, S., Suleski, M., Craig, J. M., Kasprowicz, A. E., Sanderford, M., Li, M., Stecher, G., & Hedges, S. B. (2022). TimeTree 5: An expanded resource for species divergence times. *Molecular Biology and Evolution*, 39(8), msac174.

Lin, J.-J., Wang, F.-Y., Chung, W.-Y., & Wang, T.-Y. (2024). The genomic evolution of visual opsin genes in amphibians. *Vision Research*, 222, 108447.

Lin, J.-J., Wang, F.-Y., Li, W.-H., & Wang, T.-Y. (2017). The rises and falls of opsin genes in 59 ray-finned fish genomes and their implications for environmental adaptation. *Scientific Reports*, 7(1), 15568.

Love, M. I., Huber, W., & Anders, S. (2014). Moderated estimation of fold change and dispersion for RNA-seq data with DESeq2. *Genome Biology*, 15(12), 550.

Luehrmann, M., Carleton, K. L., Cortesi, F., Cheney, K. L., & Marshall, N. J. (2019). Cardinalfishes (Apogonidae) show visual system adaptations typical of nocturnally and diurnally active fish. *Molecular Ecology*, 28(12), 3025–3041.

Luo, D.-G., Yue, W. W. S., Ala-Laurila, P., & Yau, K.-W. (2011). Activation of visual pigments by light and heat. *Science*, 332(6035), 1307–1312.

Maciel, A. O., & Hoogmoed, M. S. (2011). Taxonomy and distribution of caecilian amphibians (Gymnophiona) of Brazilian Amazonia, with a key to their identification. *Zootaxa*, 2984(1), 1–53.

Maddison, W. P., & Maddison, D. R. (2015). *Mesquite: a modular system for evolutionary analysis*. http://mesquiteproject.org

Makino, C. L., & Dodd, R. L. (1996). Multiple visual pigments in a photoreceptor of the salamander retina. *The Journal of General Physiology*, 108(1), 27–34.

Margetts, B. M., Stuart-Fox, D., & Franklin, A. M. (2024). Red vision in animals is broadly associated with lighting environment but not types of visual task. *Ecology and Evolution*, 14(2), e10899.

Meredith, R. W., Gatesy, J., Emerling, C. A., York, V. M., & Springer, M. S. (2013). Rod monochromacy and the coevolution of cetacean retinal opsins. *PLoS Genetics*, 9(4), e1003432.

Mohun, S. M., Davies, W. L., Bowmaker, J. K., Pisani, D., Himstedt, W., Gower, D. J., Hunt, D. M., & Wilkinson, M. (2010). Identification and characterization of visual pigments in caecilians (Amphibia: Gymnophiona), an order of limbless vertebrates with rudimentary eyes. *The Journal of Experimental Biology*, 213(20), 3586–3592.

Mohun, S. M., & Wilkinson, M. (2015). The eye of the caecilian *Rhinatrema bivittatum* (Amphibia: Gymnophiona: Rhinatrematidae). *Acta Zoologica* , 96(2), 147–153.

Murrell, B., Moola, S., Mabona, A., Weighill, T., Sheward, D., Kosakovsky Pond, S. L., & Scheffler, K. (2013). FUBAR: a fast, unconstrained bayesian approximation for inferring selection. *Molecular Biology and Evolution*, 30(5), 1196–1205.

Musilova, Z., Salzburger, W., & Cortesi, F. (2021). The visual opsin gene repertoires of teleost fishes: Evolution, ecology, and function. *Annual Review of Cell and Developmental Biology*, 37(1), 441–468.

Musser, J. M., & Arendt, D. (2017). Loss and gain of cone types in vertebrate ciliary

photoreceptor evolution. *Developmental Biology*, 431(1), 26–35.

Nevo, E. (1979). Adaptive Convergence and Divergence of Subterranean Mammals. *Annual Review of Ecology and Systematics*, 10, 269–308.

Nilsson, S. E. (1964). An electron microscopic classification of the retinal receptors of the leopard frog (Rana pipiens). *Journal of Ultrastructure Research*, *10*(5-6), 390–416.

Nishikawa, K., Matsui, M., Yoshikawa, N., Khonsue, W., & Sanamxay, D. (2021). *Ichthyophis bannanicus Yang, 1984, a junior subjective synonym of I. kohtaoensis Taylor, 1960 (Amphibia, Gymnophiona, Ichthyophiidae)*. 38(1-4), 1–17.

Ovchinnikov, V., Uliano-Silva, M., Wilkinson, M., Wood, J., Smith, M., Oliver, K., Sims, Y., Torrance, J., Suh, A., McCarthy, S. A., Durbin, R., & O'Connell, M. J. (2023). Caecilian genomes reveal the molecular basis of adaptation and convergent evolution of limblessness in snakes and caecilians. *Molecular Biology and Evolution*, 40(5).

Palczewski, K., Kumasaka, T., Hori, T., Behnke, C. A., Motoshima, H., Fox, B. A., Le Trong, I., Teller, D. C., Okada, T., Stenkamp, R. E., Yamamoto, M., & Miyano, M. (2000). Crystal structure of rhodopsin: A G protein-coupled receptor. *Science*, 289(5480), 739–745.

Patro, R., Duggal, G., Love, M. I., Irizarry, R. A., & Kingsford, C. (2017). Salmon provides fast and bias-aware quantification of transcript expression. *Nature Methods*, 14(4), 417–419.

Prakash, A., Gower, D. J., Vengot, R., & Kotharambath, R. (2024). Circadian rhythm and surface activity in soil-dwelling caecilians (Amphibia: Gymnophiona). *Scientific Reports*, 14(1), 9950.

Revell, L. J. (2024). phytools 2.0: an updated R ecosystem for phylogenetic comparative methods (and other things). *PeerJ*, 12, e16505.

Rice, P., Longden, I., & Bleasby, A. (2000). EMBOSS: The European Molecular Biology Open

Software Suite. *Trends in Genetics: TIG*, 16(6), 276–277.

Sadier, A., Sears, K. E., & Womack, M. (2022). Unraveling the heritage of lost traits. *Journal of Experimental Zoology. Part B, Molecular and Developmental Evolution*, 338(1-2), 107–118.

San Mauro, D., Gower, D. J., Müller, H., Loader, S. P., Zardoya, R., Nussbaum, R. A., & Wilkinson, M. (2014). Life-history evolution and mitogenomic phylogeny of caecilian amphibians. *Molecular Phylogenetics and Evolution*, 73(1), 177–189.

Santos, R. O., Laurin, M., & Zaher, H. (2020). A review of the fossil record of caecilians (Lissamphibia: Gymnophionomorpha) with comments on its use to calibrate molecular timetrees. *Biological Journal of the Linnean Society. Linnean Society of London*, 131(4), 737–755.

Schott, R. K., Bell, R. C., Loew, E. R., Thomas, K. N., Gower, D. J., Streicher, J. W., & Fujita, M. K. (2022). Transcriptomic evidence for visual adaptation during the aquatic to terrestrial metamorphosis in leopard frogs. *BMC Biology*, 20(1), 138.

Schott, R. K., Fujita, M. K., Streicher, J. W., Gower, D. J., Thomas, K. N., Loew, E. R., Bamba Kaya, A. G., Bittencourt-Silva, G. B., Guillherme Becker, C., Cisneros-Heredia, D., Clulow, S., Davila, M., Firneno, T. J., Jr, Haddad, C. F. B., Janssenswillen, S., Labisko, J., Maddock, S. T., Mahony, M., Martins, R. A., … Bell, R. C. (2024). Diversity and Evolution of Frog Visual Opsins: Spectral Tuning and Adaptation to Distinct Light Environments. *Molecular Biology and Evolution*, 41(4), msae049.

Taylor, E. H. (1968). *The caecilians of the world*. University of Kansas Press.

Taylor, E. H. (1969). A new Panamanian caecilian. *The University of Kansas Science Bulletin*, 48(12), 315–323.

Tettamanti, V., de Busserolles, F., Lecchini, D., Marshall, N. J., & Cortesi, F. (2019). Visual system development of the spotted unicornfish, *Naso brevirostris* (Acanthuridae). *The Journal of Experimental Biology*, 222(Pt 24), jeb209916.

Torres-Sánchez, M., Creevey, C. J., Kornobis, E., Gower, D. J., Wilkinson, M., & San Mauro, D. (2019). Multi-tissue transcriptomes of caecilian amphibians highlight incomplete knowledge of vertebrate gene families. *DNA Research: An International Journal for Rapid Publication of Reports on Genes and Genomes*, 26(1), 13–20.

Tovar, R. U., Cantu, V., Fremaux, B., Gonzalez, P., Jr, Spikes, A., & García, D. M. (2021). Comparative development and ocular histology between epigean and subterranean salamanders (Eurycea) from central Texas. *PeerJ*, 9, e11840.

Veilleux, C. C., & Cummings, M. E. (2012). Nocturnal light environments and species ecology: implications for nocturnal color vision in forests. *The Journal of Experimental Biology*, 215(23), 4085–4096.

Vidal-García, M., Byrne, P. G., Roberts, J. D., & Keogh, J. S. (2014). The role of phylogeny and ecology in shaping morphology in 21 genera and 127 species of Australo-Papuan myobatrachid frogs. *Journal of Evolutionary Biology*, 27(1), 181–192.

Wake, M. H. (1985). The comparative morphology and evolution of the eyes of caecilians (Amphibia, Gymnophiona). *Zoomorphology*, 105(5), 277–295.

Wake, M. H. (1993). Non-traditional characters in the assessment of caecilian phylogenetic relationships. *Herpetological Monograph*, 7, 42.

Walls, G. L. (1942). *The vertebrate eye and its adaptive radiation [by] Gordon Lynn Walls*. Cranbrook Institute of Science,.

Wan, Y. C., Navarrete Méndez, M. J., O'Connell, L. A., Uricchio, L. H., Roland, A.-B., Maan,

M. E., Ron, S. R., Betancourth-Cundar, M., Pie, M. R., Howell, K. A., Richards-Zawacki, C. L., Cummings, M. E., Cannatella, D. C., Santos, J. C., & Tarvin, R. D. (2023). Selection on visual opsin genes in diurnal Neotropical frogs and loss of the SWS2 opsin in poison frogs. *Molecular Biology and Evolution*, 40(10), msad206.

Warrant, E. (2000). The eyes of deep-sea fishes and the changing nature of visual scenes with depth. *Philosophical Transactions of the Royal Society of London. Series B, Biological Sciences*, 355(1401), 1155–1159.

Weadick, C. J., & Chang, B. S. W. (2012). An improved likelihood ratio test for detecting site-specific functional divergence among clades of protein-coding genes. *Molecular Biology and Evolution*, 29(5), 1297–1300.

Wertheim, J. O., Murrell, B., Smith, M. D., Kosakovsky Pond, S. L., & Scheffler, K. (2015). RELAX: detecting relaxed selection in a phylogenetic framework. *Molecular Biology and Evolution*, 32(3), 820–832.

Yang, Z. (2007). PAML 4: phylogenetic analysis by maximum likelihood. *Molecular Biology and Evolution*, 24(8), 1586–1591.

Yokoyama, S. (2002). Molecular evolution of color vision in vertebrates. *Gene* 300, 69–78.

Yokoyama, S., & Radlwimmer, F. B. (2001). The molecular genetics and evolution of red and green color vision in vertebrates. *Genetics*, 158, 1697–1710.

Yovanovich, C. A. M., Koskela, S. M., Nevala, N., Kondrashev, S. L., Kelber, A., & Donner, K. (2017). The dual rod system of amphibians supports colour discrimination at the absolute visual threshold. *Philosophical Transactions of the Royal Society of London. Series B, Biological Sciences*, 372(1717), 20160066.